

Towards Metric GPR Migration based on DNN Noise Removal and Dielectric Estimation

Jinglun Feng¹, Liang Yang¹, Jizhong Xiao^{1*} *Senior Member, IEEE*

Abstract—Ground Penetrating Radar (GPR) is one of the most important non-destructive evaluation (NDE) devices to detect the subsurface objects (i.e. rebars, utility pipes) and reveal the underground scene. Due to the background noise and unknown dielectric property of GPR data, the reconstruction of the subsurface objects with metric information remains the main challenge in GPR inspection. In this letter, a novel metric GPR migration method is proposed consisting of three steps to address the above challenge. Firstly, a noise removal segmentation model is introduced to clear the GPR raw data; furthermore, a DielectricNet is proposed to predict the dielectric of each GPR B-scan data and the depth of a target object; at the last step, we optimize the migration algorithm by using random motion pattern, thus to obtain the 3D metric migration result. We use both the field and synthetic data to verify the proposed method, experimental results show that our proposed method is able to achieve at least 10% improvement in reconstruction accuracy compared with the conventional migration methods.

Index Terms—Back-projection algorithm (BPA), ground penetrating radar (GPR), deep neural network, non-destructive evaluation (NDE).

I. INTRODUCTION

GROUND Penetrating Radar is widely used in non-destructive testing (NDT), field archaeology investigation, infrastructure inspection, and measurements. GPR sensing technique is based on a geophysical remote sensing method where the transmitter emits the electromagnetic (EM) wave into the subsurface and travels at a specific velocity determined by the dielectric properties, thus eventually reveal the underground objects. In the current practice of GPR inspection, an inspector carries a hand-held GPR device and using a survey wheel to scan the surface along pre-marked linear paths only. Then, experienced engineers are required to manually label objects of interest in GPR images and further interpret GPR data with migration methods to locate and map the buried objects.

However, there are two major challenges to reveal underground objects using GPR. First, to reveal the subsurface targets, current migration methods are easily being affected by several considerations, i.e., *permittivity of the material, background data noisy, the position and orientation of current GPR data*, etc., thus, to propose an efficient metric GPR migration method to avoid the above factors and allowing regular persons to understand the reconstructed subsurface objects is crucial. Secondly, it is also time-consuming and

tedious work to manually scan a large area for detailed mapping, since current commercial GPR devices can only move forward and backward while cannot make a turn. It causes the GPR data would just either be collected parallel or perpendicular with the pre-defined straight lines, which is hard to cover the data collection area as much as possible.

Many studies have devoted to the GPR migration related methods in order to map the subsurface scenes. Kirchhoff migration method is first introduced in the 1970s; according to [1], the Kirchhoff migration method is capable to focus on the target position, however, it's processing speed is slower than the rest of the migration approaches. Phase-shift migration is a mathematical-based method which is proposed in 1978 [2], it utilizes the ESM concept to focus the targets from GPR B-scan data; for comparable accuracy, this approach is computationally more efficient than the finite-difference [3] approach, which is designed for the geometry of a single radargram source with a line of surface receivers. Furthermore, the back-projection (BP) algorithm is served as the most significant and common 2D imaging reconstruction method in GPR [4], [5]. When GPR emits the radiation pulse, the BP algorithm assumes this wave path shares a semi-sphere pattern with an equal energy level. After GPR receives the radiation pulse back, the BP algorithm stack the radiation energy along the hyperbolic trajectory, then the sum of the responded amplitude could reflect the target region.

Besides the migration and perception, GPR data reconstruction methods with metric information are popular researched in recent years as well. University of Vermont's research group has published several papers [6], [7] on GPR-based reconstruction using multistatic air-coupled GPR. They first collect the data from different GPR antenna, and further take each obtained gain of GPR data into consideration; moreover, to remove the noise, they also fuse the data with a Hessian-based enhancement filter, which is novel. However, the positioning information in their reconstructed object model is not mentioned in the above methods. Similarly, Prof. Dezheng Song's group at Texas A&M University published a series of papers on automatic subsurface pipeline mapping and 3D reconstruction by fusing a GPR and a Camera [8], [9]. They proposed a robotic underground pipeline mapping model to facilitates GPR-based 3D reconstruction. The main contribution of their proposed method is that they fuse the V-SLAM readings and J-linkage and maximum likelihood method to estimate the radii and locations of all pipelines, however, the average error for pipe radius estimation is over 35%, which is not good enough for practical use [8].

In this letter, we proposed a novel GPR migration method

¹The CCNY Robotics Lab, Electrical Engineering Department, The City College of New York, New York, USA email(jfeng1, lyang1, jxiao@ccny.cuny.edu)

*Corresponding author.

that consists of a DNN model to remove GPR B-scan *background noise* and a *DielectricNet* which is able to provide metric estimation, and it is able to optimize the reconstruction by taking *random motion*. The noise removal model is to clean the noised data in a GPR B-scan, and the DielectricNet aims to predict the dielectric of subsurface materials to provide metric information for the migration process. The *random motion* method is proposed to address the issue that conventional GPR migration methods are not able to take the orientation of GPR data into consideration, and thus to enable accurate reconstruction of the subsurface targets with higher coverage.

II. METHODOLOGY

A. DNN-based GPR Target Segmentation and Depth Prediction

Due to the GPR background noise and the uncertainty of the material dielectric, it is almost impossible to reconstruct the underground objects with an accurate metric. To resolve this issue, we propose two models, which are GPR object segmentation model and dielectric prediction model, to facilitate accurate subsurface object reconstruction. The DNN networks are illustrated in Fig.1, where we use a U-Net [10] to perform subsurface object segmentation and a DielectricNet to predict the dielectric of the subsurface material.

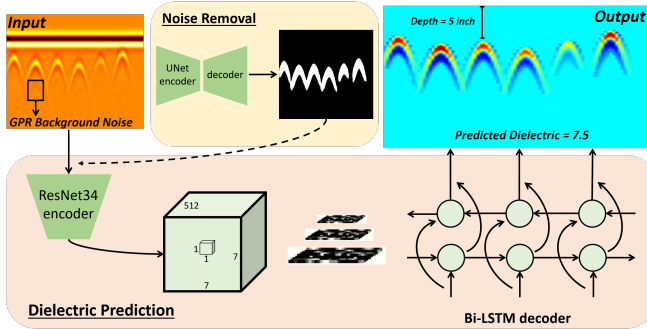


Fig. 1. The architecture of the proposed GPR noise removal model and the dielectric prediction model. For the input B-scan image, the noise removal model directly decodes the input image into a hyperbolic feature. The dielectric prediction model takes the segmentation masks from the noise removal model and pools the dielectric information out from a CRNN model.

1) *GPR Background Noise Removal*: GPR works by sending an EM wave into the ground, as the emitted pulse enters a material with different dielectric. GPR antenna would thus record the strength of each reflection as well as time it takes to return to the receiver. Therefore, when GPR surveys over an underground object, some of the GPR energy pulse reflects to receiver when they hit the subsurface object, some energy continues to penetrate through the object until they become too weak to get back. However, those weak reflections would also generate hyperbolic features in the B-scan image, which could affect the migration result of the targets. We call those weak responses as *GPR Background Noise* (see in Fig.1). Hence, it is important for us not only focusing on enhancing and sharpening B-scan features but also removing those background noise.

Specifically, we firstly get hyperbolic mask from the input raw B-scan images by taking the advantages of a segmentation

model, that is, UNet. Then, we filter the raw B-scan data with mask B-scan features so that the filtered data only keeps the strongest target reflection signal.

2) *GPR Targets Depth Prediction*: Dielectric constant is crucial for GPR migration since it determines the depth of each target in a B-scan image. As shown in Equ.2, the EM wave is supposed to be with a speed of light in vacuum. However, the dielectric \mathcal{D} of subsurface materials would make a difference to the traveling speed, which further affect the depth prediction of the target.

$$v = \frac{C}{\sqrt{\mathcal{D}}} \quad (1)$$

$$D_{tar} = \frac{T_{tr}}{2v} \quad (2)$$

where D_{tar} denotes depth of subsurface targets while T_{tr} is the two way travel time of GPR's antenna.

Thus, for any underground object, if dielectric of surrounding material is high, the B-scan hyperbolic feature would be deeper than the same target with a smaller environment dielectric. On account of this property and inspired by [11], we introduced a Convolutional Recurrent Neural Network (CRNN) model in this letter, that is, DielectricNet, to outputs the dielectric, $d_{t(i)}, i \in \{0, 1, \dots\}$ for each target.

Given a GPR scan with an unknown dielectric, an informative and discriminative feature representation plays a significant role in dielectric estimation. The feature representation should preserve the dielectric nature of the underground scene, moreover, it should consider the spatial distribution of all hyperbolic features to enable the better dielectric prediction. We take the advantage of RNN, which is able to take a sequence of signal either spatially continuous or temporally continuous, to estimate the dielectric. The encoder is ResNet34 as the encoder and an RNN model as the decoder, where the GPR image feeds into a series of convolutional layers to obtain the feature map as the output that contains encoded dielectric information [12].

In our implementation, the input noise free B-scan image is resized to 224×224 while the *ResNet34* [13] architecture changed to work in a fully convolutional manner by converting *fc6* to fully convolutional layers. Then, an *Bi-LSTM* decoder extracts dielectric property from the CNN encoded feature descriptors, where it sequentially outputs their corresponding confidence scores for the predicted dielectric value. This design helps the model to reason the dielectric perception.

Loss Design: Once predicting the depth of each target and the dielectric, we optimize the model by using a Connectionist Temporal Categorical (CTC) loss.

$$\sum_i P(D | \mathbf{x}) = \sum_i P(D | \pi_i) P(\pi_i | x) \quad (3)$$

where D is the ground truth depth, \mathbf{x} is the input sequence that comes from RNN model, and π_i denotes each possible value of the dielectric.

B. GPR Migration with 3D Metric

A conventional migration process is usually composed of the following steps:

- Background Removal (remove the direct coupling area between GPR transmitter and the ground surface)
- Target Depth Estimation
- Back Projection Processing

Notice that step 1 and 2 are solved in Section.II-A1, thus, in order to create a 3D migration model, back projection (BP), as one of the most representative GPR imaging algorithms, is widely used in industry. As we discussed in the previous section, the essence of A-scan represents amplitude of EM energy, while BP is a process of aggregation that converts different amplitude of energy into a *semi-sphere* format at different depth. As illustrated in Fig.2, the brighter semi-sphere indicates the higher amplitude part in A-scan. Furthermore, the radius of each semi-sphere in BP image indicates the depth between the ground and the object, which is calculated by Equ.2. To implement the BP algorithm, we firstly need to correct *time-zero* to adjust the response where *time-zero* represents the first reflection from the surface of the ground, the correction process is illustrated as in Equ.4.

$$\overline{A}_p^k = \frac{\sum_{i=1}^q A_{q,p}^k}{q} \quad (4)$$

where \overline{A}_p^k presents the mean *time-zero* of all A-scans, and $A_{q,p}^k = \{a_t | t = p, p \in \{1, q\}\}$ is the *first peak* in the q -th A-scan measurement of the k -th B-scan data, which also represents the amplitude corresponds to response of the surface of ground.

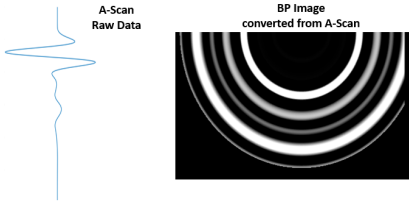


Fig. 2. BP algorithm converts the A-scan raw data into a set of semi-spheres.

Once we correct the *time-zero* of all A-scans, we can back-project the A-scans as discussed in Equ.5 [8],

$$\forall A_q^k \in B_k, (x-a)^2 + (y-b)^2 = (a_t * t)^2, y < 0 \quad (5)$$

where a, b represents the specific position of each A-scan measurement in a slab. $A_q^k = \{a_t | t = 1, \dots, n_q\}$ represents the q -th A-scan measurement in k -th B-scan data, while t and a_t indicate the traveling time and amplitude of A-scan signal respectively, then n_q means the total samples in a A-scan measurements. Meanwhile, we also have $B_k = \{A_q^k | q = 1, \dots, n_k\}$ that represents the k -th B-scan consisting of n_k A-scans. By implementing the BP algorithm on a B-scan data, the intersection of multiple back-projected A-scan signals with the highest energy level is the possible target location.

Random Motion Based Optimization: However, conventional migration methods still rely on the wheel encoder that only support linear motion without rotation, the GPR data collected by the conventional method only covers either the horizontal or perpendicular directions. These measurements

heavily rely on the consistency of orientation and limit the coverage of the inspection. To solve this problem, we propose a real 3D metric migration method which implements the *random-motion* data collection pattern. Instead of relying on linear wheel encoder, we use an RGB-D camera to estimate the position and orientation on-the-fly which is mentioned in our previous works [14], [15]. Thus, by receiving positioning and rotation information from our pose estimation system, the GPR cart is able to collect the GPR data in any directions, and thus constructs real 3D GPR image. In Equ.6, P_{pre} denotes the position of previous GPR antenna while P_{update} represents the coordinate of updated GPR antenna. θ is the rotation angle of the GPR device.

$$\begin{bmatrix} P_{update_x} \\ P_{update_y} \end{bmatrix} = \begin{bmatrix} \cos \theta & -\sin \theta \\ \sin \theta & \cos \theta \end{bmatrix} \times \begin{bmatrix} P_{pre_x} \\ P_{pre_y} \end{bmatrix} \quad (6)$$

III. EXPERIMENTS STUDY

To demonstrate the effectiveness of the proposed 3D metric migration method, we conducted both simulations and laboratory experiments. The synthetic data were generated by gprMax [16] while the laboratory data were collected on a concrete slab at CCNY Robotics Lab Testing Pit, River Edge, NJ, USA. We also compare the effectiveness between proposed method and others in this section, and discuss the effectiveness of the DethpNet model. All these evaluations are conducted on an GPU server, with Intel Core i9-9900K 3.2GHz CPU, GeForce RTX 2080 Ti GPU, and 32GB RAM.

A. Data Sets Description and 3D Metric Migration Effectiveness Study

In order to create the dataset for experimental purpose, we collected two kinds of data: 1) the field data collected on CCNY Testing Pit, which contains 120 B-scan data; 2) synthetic data that we proposed in [18], and it contains 628 B-scan data. Note that all the B-scan images are taken as the input for noise cancellation and dielectric prediction task, and then used to verify the proposed migration method.

As illustrated in Fig.3, both synthetic and field GPR data has been used for the validation of the effectiveness of proposed migration method. Specifically, Fig.3(a) shows a synthetic slab which is 1.3m meters long and 0.25 meters deep. In addition, Fig.3(b) shows the ground truth of the field experimental slab, noticed the black bounding box showing in the (b) demonstrates the field GPR data collection area, where has the 1.55 meters long and 0.2 meters deep. Then, Fig. 3(c) to (f) shows the raw B-scan data and noise removed B-scan data respectively. At last, Fig.3(g) and (h) shows the proposed metric migration results.

B. Comparison and Analysis of the 3D Metric Migration Method

1) *Migration Results Comparison:* To further validate the proposed method, we further compare the 3D metric migration with conventional back-projection based migration method [17] and another DNN-based migration method proposed in

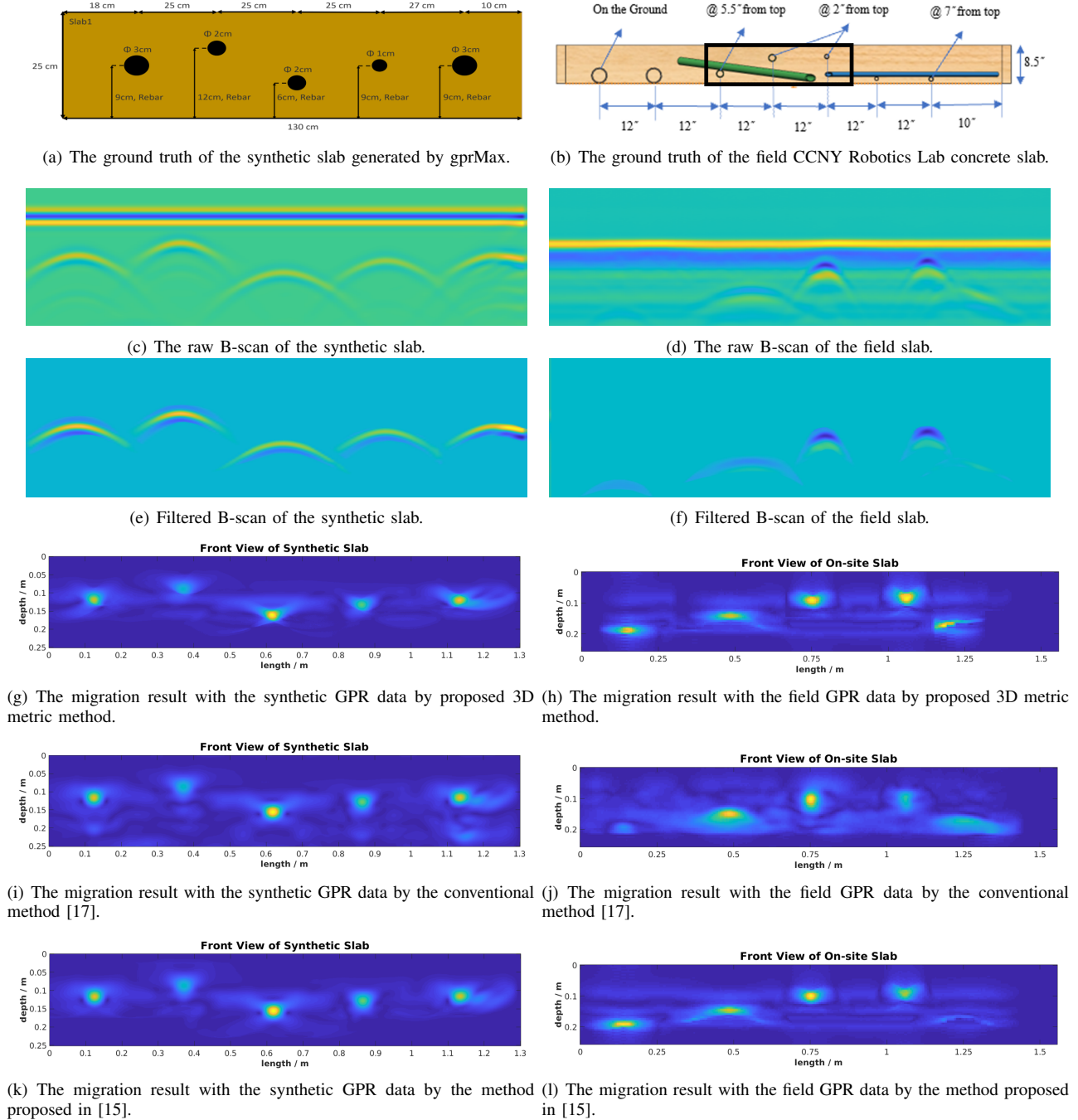


Fig. 3. Effectiveness and noise comparison of proposed migration method on both synthetic and field GPR data, all the migration results are shown with a front view. Note that in subfigure (b), the black bounding box demonstrates the field data collection area.

[15], where they remove the noise in B-scan data by a hyperbolic feature detection network. As illustrated in Fig.3(g)-(l), we demonstrate migration results by the above methods respectively. Specifically, (i) and (j) shows that the conventional migration results which contain too much noisy data while in subfigure (k) and (l), the noise is removed and the migration result is getting better. However, the effect in (k) and (l) is still not as good as the proposed method in this letter, as demonstrated in Table.II, the image noise level and similarity effectiveness is evaluated with the with four different metrics, that is, *Euclidean Distance*, *Mean Square Error*, *Signal-to-Noise-Ratio* and *Structural Similarity Index*, on both synthetic

dataset and field dataset. Specifically, for *Euclidean Distance* and *Mean Square Error*, the lower the value is, the better the performance is while for metric *Signal-to-Noise-Ratio* and *Structural Similarity Index*, the larger the value is, the better effectiveness it represents.

The reason is that a segmentation model could capture the shape of the hyperbolic feature, which contains all the useful information in a B-scan data, while for the information in the bounding box region generated by the detection oriented model, it would contain some noise data besides the useful B-scan data as well.

TABLE I
EFFECTIVENESS COMPARISON BETWEEN PROPOSED METHOD AND OTHERS WITH MULTIPLE METRICS

	E_distance	MSE	SNR	SSMI
Ours w/ synthetic dataset	2.23e+04	284.774	16.982	0.987
[17] w/ synthetic dataset	4.05e+04	351.455	16.068	0.976
[15] w/ synthetic dataset	9.08e+04	453.541	14.961	0.983
Ours w/ field dataset	1.39e+03	397.384	15.810	0.980
[15] w/ field dataset	1.92e+03	485.132	14.943	0.971
[17] w/ field dataset	3.40e+03	983.156	11.876	0.938

2) *Why CRNN model works for dielectric prediction?:* In this letter, there is another interesting topic, that is, why a CRNN model works for the dielectric prediction task. It is known that CRNN model is used for the *image-based sequence recognition* task, obviously, there is no any sequences in a B-scan image. However, served as one of an essential properties in GPR data, the dielectric value depicts B-scan image in another way, which is the depth of each hyperbolic features in a B-scan image. Therefore, we can encode this property as an abstract sequence, since with the same objects and other conditions in the different underground environments, their B-scan image would be different if the dielectric changes. Due to the above reason, we implement a CRNN model in this letter to predict this abstract property as a *sequence*, where the CNN encoder we implement is *ResNet34* and the RNN decoder is *Bi-LSTM*. In addition, different methods, which is a CRNN model with *VGG16* encoder and *Bi-LSTM* decoder and a single *ResNet34* network [15] respectively, to predict dielectric value are illustrated by comparing their prediction accuracy and running time, since the loss function in each method is not the same. As shown in Tabel.II, the CRNN model implemented in this letter gains at least 0.7% better prediction accuracy and 30% faster respectively.

TABLE II
PERFORMANCE COMPARISON BETWEEN PROPOSED METHOD AND OTHERS

	Ours	VGG16 + Bi-LSTM	ResNet34
Acc.	98.29	97.56	98.05
Time(sec.)	0.0049	0.0065	0.0075

IV. CONCLUSION

This paper introduces a DNN-based 3D metric migration method, which is able to enhance the conventional migration performance by taking the following steps: 1) using a segmentation model to remove the background noised from raw GPR B-scan; 2) using DielectricNet to estimate the dielectric value for different underground environment; 3) improve the back projection method by using a random motion pattern. Comparative experiment results shows our proposed method could recover a more concentrated target compared to the conventional approaches with a higher accuracy.

ACKNOWLEDGMENT

Financial support for this study was provided by NSF grant IIP-1915721, and by the U.S. Department of Transportation,

Office of the Assistant Secretary for Research and Technology (USDOT/OST-R) under Grant No. 69A3551747126 through INSPiRE University Transportation Center (<http://inspire-utc.mst.edu>) at Missouri University of Science and Technology. J Xiao has significant financial interest in InnovBot LLC, a company involved in R&D and commercialization of the technology.

REFERENCES

- [1] N. Smitha, D. U. Bharadwaj, S. Abilash, S. Sridhara, and V. Singh, "Kirchhoff and fk migration to focus ground penetrating radar images," *International Journal of Geo-Engineering*, vol. 7, no. 1, p. 4, 2016.
- [2] J. Gazdag, "Wave equation migration with the phase-shift method," *Geophysics*, vol. 43, no. 7, pp. 1342–1351, 1978.
- [3] J. F. Claerbout and S. M. Doherty, "Downward continuation of moveout-corrected seismograms," *Geophysics*, vol. 37, no. 5, pp. 741–768, 1972.
- [4] S. Demirci, H. Cetinkaya, E. Yigit, C. Ozdemir, and A. A. Vertiy, "A study on millimeter-wave imaging of concealed objects: Application using back-projection algorithm," *Progress In Electromagnetics Research*, vol. 128, pp. 457–477, 2012.
- [5] S. Demirci, E. Yigit, I. H. Eskidemir, and C. Ozdemir, "Ground penetrating radar imaging of water leaks from buried pipes based on back-projection method," *Ndt & E International*, vol. 47, pp. 35–42, 2012.
- [6] M. Pereira, Y. Zhang, D. Orfeo, D. Burns, D. Huston, and T. Xia, "3d tomographic image reconstruction for multistatic ground penetrating radar," in *2019 IEEE Radar Conference (RadarConf)*. IEEE, 2019, pp. 1–6.
- [7] M. Pereira, D. Burns, D. Orfeo, Y. Zhang, L. Jiao, D. Huston, and T. Xia, "3-d multistatic ground penetrating radar imaging for augmented reality visualization," *IEEE Transactions on Geoscience and Remote Sensing*, 2020.
- [8] H. Li, C. Chou, L. Fan, B. Li, D. Wang, and D. Song, "Toward automatic subsurface pipeline mapping by fusing a ground-penetrating radar and a camera," *IEEE Transactions on Automation Science and Engineering*, vol. 17, no. 2, pp. 722–734, 2019.
- [9] —, "Robotic subsurface pipeline mapping with a ground-penetrating radar and a camera," in *2018 IEEE/RSJ International Conference on Intelligent Robots and Systems (IROS)*. IEEE, 2018, pp. 3145–3150.
- [10] O. Ronneberger, P. Fischer, and T. Brox, "U-net: Convolutional networks for biomedical image segmentation," in *International Conference on Medical image computing and computer-assisted intervention*. Springer, 2015, pp. 234–241.
- [11] B. Shi, X. Bai, and C. Yao, "An end-to-end trainable neural network for image-based sequence recognition and its application to scene text recognition," *IEEE Transactions on Pattern Analysis and Machine Intelligence*, vol. 39, no. 11, pp. 2298–2304, 2017.
- [12] X. Rong, C. Yi, and Y. Tian, "Unambiguous text localization and retrieval for cluttered scenes," in *Proceedings of the IEEE Conference on Computer Vision and Pattern Recognition*, 2017, pp. 5494–5502.
- [13] K. He, X. Zhang, S. Ren, and J. Sun, "Deep residual learning for image recognition," in *Proceedings of the IEEE conference on computer vision and pattern recognition*, 2016, pp. 770–778.
- [14] L. Yang, Y. Chang, S. Sotnikov, J. Feng, B. Li, and J. Xiao, "Wind-turbine blade inspection using impact-sounding module and acoustic analysis," in *2019 IEEE 9th Annual International Conference on CYBER Technology in Automation, Control, and Intelligent Systems (CYBER)*, 2019, pp. 253–258.
- [15] J. Feng, L. Yang, H. Wang, Y. Song, and J. Xiao, "Gpr-based subsurface object detection and reconstruction using random motion and depthnet," in *2020 IEEE International Conference on Robotics and Automation (ICRA)*. IEEE, 2020, pp. 7035–7041.
- [16] C. Warren, A. Giannopoulos, and I. Giannakis, "gprmax: Open source software to simulate electromagnetic wave propagation for ground penetrating radar," *Computer Physics Communications*, vol. 209, pp. 163–170, 2016.
- [17] X. Xie, J. Zhai, and B. Zhou, "Back-fill grouting quality evaluation of the shield tunnel using ground penetrating radar with bi-frequency back projection method," *Automation in Construction*, vol. 121, p. 103435, 2021.
- [18] J. Feng, L. Yang, H. Wang, Y. Tian, and J. Xiao, "Subsurface pipes detection using dnn-based back projection on gpr data," in *Proceedings of the IEEE/CVF Winter Conference on Applications of Computer Vision (WACV)*, January 2021, pp. 266–275.